Preconditioning of Arctic Stratospheric Polar Vortex Shift Events

Article *in* Journal of Climate · April 2018

DOI: 10.1175/JCLI-D-17-0695.1

CITATIONS
0

READS
229

7 authors, including:

Jinlong Huang
Lanzhou University
8 PUBLICATIONS **71** CITATIONS
SEE PROFILE

Wenshou Tian
University of Leeds
120 PUBLICATIONS **2,782** CITATIONS
SEE PROFILE

L. J. Gray
University of Oxford
186 PUBLICATIONS **7,871** CITATIONS
SEE PROFILE

Jiankai Zhang
Lanzhou University
38 PUBLICATIONS **221** CITATIONS
SEE PROFILE

Preconditioning of Arctic Stratospheric Polar Vortex Shift Events

JINLONG HUANG AND WENSHOU TIAN

Key Laboratory for Semi-Arid Climate Change of the Ministry of Education, College of Atmospheric Sciences, Lanzhou University, Lanzhou, China

LESLEY J. GRAY

National Centre for Atmospheric Science, Physics Department, University of Oxford, Oxford, United Kingdom

JIANKAI ZHANG, YAN LI, JIALI LUO, AND HONGYING TIAN

Key Laboratory for Semi-Arid Climate Change of the Ministry of Education, College of Atmospheric Sciences, Lanzhou University, Lanzhou, China

(Manuscript received 19 October 2017, in final form 23 March 2018)

ABSTRACT

This study examines the preconditioning of events in which the Arctic stratospheric polar vortex shifts toward Eurasia (EUR events), North America (NA events), and the Atlantic (ATL events) using composite analysis. An increase in blocking days over northern Europe and a decrease in blocking days over the Bering Strait favor the movement of the vortex toward Eurasia, while the opposite changes in blocking days over those regions favor the movement of the vortex toward North America. An increase in blocking days over the eastern North Atlantic and a decrease in blocking days over the Bering Strait are conducive to movement of the stratospheric polar vortex toward the Atlantic. These anomalous precursor blocking patterns are interpreted in terms of the anomalous zonal wave-1 or wave-2 planetary wave fluxes into the stratosphere that are known to influence the vortex position and strength. In addition, the polar vortex shift events are further classified into events with small and large polar vortex deformation, since the two types of events are likely to have a different impact at the surface. A significant difference in the zonal wave-2 heat flux into the lower stratosphere exists prior to the two types of events and this is linked to anomalous blocking patterns. This study further defines three types of tropospheric blocking events in which the spatial patterns of blocking frequency anomalies are similar to the blocking patterns prior to EUR, NA, and ATL events, respectively, and our reanalysis reveals that the polar vortex is indeed more likely to shift toward Eurasia, North America, and the Atlantic in the presence of the above three defined tropospheric blocking events. These shifts of the polar vortex toward Eurasia, North America, and the Atlantic lead to statistically significant negative height anomalies near the tropopause and corresponding surface cooling anomalies over these three regions.

1. Introduction

Previous studies have shown that the stratospheric polar vortex plays a critical role in the interaction between the stratosphere and troposphere (e.g., Baldwin and Dunkerton 1999, 2001; Thompson et al. 2002; Charlton and Polvani 2007; Kidston et al. 2015; Martineau and Son 2015; Xie et al. 2016; Zhang et al. 2016). Variations in the stratospheric polar vortex can extend downward into the troposphere and affect the tropospheric jet streams (Baldwin and Dunkerton 1999), storm tracks (Baldwin and Dunkerton 2001; Limpasuvan et al. 2004, 2005), and surface weather (e.g., Kuroda 2008; Kolstad et al. 2010; Wang and Chen 2010; Woollings et al. 2010; Mitchell et al. 2013; Davini et al. 2014). Specifically, sudden stratospheric warmings (SSWs), which are characterized by a dramatic weakening of the stratospheric polar vortex and a rapid temperature increase in the polar region (Matsuno 1970), are precursors of cold air outbreaks at midlatitudes in the Northern Hemisphere (Mitchell et al. 2013; Hitchcock and Simpson 2014; Nath et al. 2016). In

Supplemental information related to this paper is available at the Journals Online website: https://doi.org/10.1175/JCLI-D-17-0695.s1.

Corresponding author: Wenshou Tian, wstian@lzu.edu.cn

DOI: 10.1175/JCLI-D-17-0695.1

addition to the influence of variability in the strength of the stratospheric polar vortex on tropospheric weather, variations in its geometry and position can exert an important impact on tropospheric weather. Charlton and Polvani (2007) classified SSWs into displacement SSWs characterized by a stratospheric polar vortex displaced far from the pole and split SSWs characterized by a split stratospheric polar vortex. Subsequently, many studies have focused on the response of tropospheric weather and climate to the two types of SSWs (Mitchell et al. 2013; Seviour et al. 2013, 2016; Maycock and Hitchcock 2015). Mitchell et al. (2013) found that the two types have different impacts on tropospheric weather and climate. Seviour et al. (2013) further indicated that split SSWs are followed by a negative Arctic Oscillation surface pattern, while displacement SSWs lead to smaller surface anomalies. Recent studies have noted that over the past three decades, the average location of the stratospheric polar vortex has shifted away from the North Pole and toward the Eurasian continent (Zhang et al. 2016, 2018; Garfinkel et al. 2017; Seviour 2017). Zhang et al. (2016) further indicated that this shift has resulted in lower temperatures over some parts of the Eurasian continent and North America in late winter and early spring. Identifying potential precursors or preconditions for the shift of the stratospheric polar vortex toward different regions is therefore important not only for predicting the location of the stratospheric polar vortex, but also for its potential downward influence on surface weather.

Previous studies have regarded the vertically propagating planetary waves from the troposphere and their subsequent evolution as predominant precursors of stratospheric polar vortex variability (e.g., Charney and Drazin 1961; Matsuno 1970; Limpasuvan et al. 2004, 2005; Polvani and Waugh 2004; Kolstad and Charlton-Perez 2011; Bancalá et al. 2012; Martineau and Son 2013, 2015; Attard et al. 2016). However, this tropospheric forcing of stratospheric variability is neither linear nor one-way. The propagation and evolution of the waves once they enter the stratosphere, and hence their impact on the polar vortex, depends on the background state of the stratosphere (Scott and Polvani 2004; Matthewman and Esler 2011; Hitchcock and Haynes 2016; Cámara et al. 2017). Any resulting changes in the polar vortex strength, location, and shape can, in turn, extend deep into the polar lower stratosphere and thence to the surface, affecting not only the source of the tropospheric wave forcing but also the longevity of weather patterns associated with it.

Moreover, many studies reported that the different wave activity precursors can lead to different types of variations in the stratospheric polar vortex geometry (e.g., Charlton and Polvani 2007; Castanheira and Barriopedro 2010). Charlton and Polvani (2007) indicated that enhanced planetary waves of zonal wave 1 can lead to a displaced polar vortex, but the split polar vortex is related to anomalous planetary wave activity of zonal wave 2 entering the stratosphere. Furthermore, Castanheira and Barriopedro (2010) found that the enhanced zonal wave 2 cannot reduce the strength of the stratospheric polar vortex and even leads to acceleration of the polar vortex; however, an enhanced zonal wave 2 preceded by an amplification of zonal wave 1 can force the polar vortex to split.

A variety of tropospheric factors have also been shown to significantly impact the stratospheric planetary wave patterns. These include external forcing factors such as Arctic sea ice (Kim et al. 2014; Zhang et al. 2016), Eurasian snow cover (Cohen and Fletcher 2007; Smith et al. 2010), and tropical sea surface temperature (Taguchi and Hartmann 2006; Garfinkel and Hartmann 2008; Barriopedro and Calvo 2014; Iza and Calvo 2015; Li and Tian 2017; Polvani et al. 2017). In addition, internal atmospheric processes, such as teleconnection patterns (e.g., Dai and Tan 2016; Bao et al. 2017; Li et al. 2018) and tropospheric blocking (e.g., Quiroz 1986; Mukougawa and Hirooka 2004; Martius et al. 2009; Castanheira and Barriopedro 2010; Nishii et al. 2010, 2011; Woollings et al. 2010; Huang et al. 2017), are known potential precursors of stratospheric polar vortex variability. Specifically, there is a distinct geographical dependence of the impact of tropospheric blocking on upward planetary wave propagation. Martius et al. (2009) demonstrated that geographical differences in blocking patterns can lead to different types of SSWs. However, a question that has not been addressed in previous studies is whether different patterns of tropospheric blockings can lead to different stratospheric polar vortex spatial positions and orientations.

In this study, we define three types of polar vortex shift events and examine precursors of stratospheric polar vortex movement toward Eurasia, North America, and the Atlantic, based on tropospheric blocking patterns. Note that the study considers all displacement events, regardless of whether or not the displacement leads to the complete breakdown of the vortex as in SSWs. The paper is structured as follows: section 2 describes the data and methodology used in this work; sections 3 describes main stratospheric characteristics of polar vortex shift events; section 4 describes associated planetary-scale wave anomalies; and section 5 explores the links to tropospheric blocking patterns and the impact of the polar vortex shift events on the troposphere. A summary of the main results is presented in section 6.

2. Data and method

The European Centre for Medium-Range Weather Forecasts (ECMWF) interim reanalysis (ERA-Interim; ECMWF 2009; Dee et al. 2011) dataset from 1979 to 2015 is used in this study. The daily surface air temperature has a horizontal resolution of 1° × 1° and the daily mean geopotential height, wind, and temperature fields have a horizontal resolution of 1° × 1° and 37 pressure levels from 1000 hPa to 1 hPa. The potential vorticity (PV) data have a horizontal resolution of 1.5° × 1.5° and are on 15 isentropic levels from 265 to 850 K. Only winter (December–February) is used to define the stratospheric polar vortex shift events in this study. The anomalies presented in this study are formed by subtracting the daily climatological annual cycle from the data at all time steps.

To investigate the precondition of anomalies in stratospheric polar vortex position, we first define the stratospheric polar vortex edge. Following Nash et al. (1996), the stratospheric polar vortex edge is defined as the equivalent latitude of maximum PV gradient in the region of the maximum westerly wind. Next, we select four key areas of Eurasia (45°–75°N, 0°–120°E), the Pacific (45°–75°N, 150°E–150°W), North America (45°–75°N, 135°–60°W), and the Atlantic (45°–75°N, 60°W–0°) to detect the shifts in the geographical location of the stratospheric polar vortex; the fractional area covered by the vortex over the four selected regions is calculated based on the method of Zhang et al. (2016). The fractional area is defined as the area of the stratospheric polar vortex covering a region divided by the total vortex area. The stratospheric polar vortex shift events toward Eurasia (EUR events) are regarded as the shifted polar vortex centered over Eurasia when the following conditions are fulfilled.

First, the fractional area covering Eurasia on the 850-K isentropic surface is larger than the fractional areas over the other three regions. Second, the fractional area covering Eurasia is larger than its daily climatology value, and the fractional areas over the other three regions are less than their daily climatology values. Third, the shifted polar vortex has only one vortex center defined as the location of the maximum value of the PV field on the 850-K isentropic surface, which precludes a split polar vortex. Note that we also examine the stratospheric polar vortex shift events on the 700- and 600-K isentropic surfaces, but the defined events among the three isentropic surfaces differ only slightly. In the following analysis, we focus on these events on the 850-K isentropic surface because of the better-defined edge of the stratospheric polar vortex relative to those of the other two isentropic surfaces. We also show the vertical structure of the stratospheric polar vortex.

To ensure the independence of the selected events, EUR events need to be spaced at least 7 days apart. The choice of 7 days is based on the fact that the atmospheric motion of purely adiabatic flows is restricted to isentropic surfaces over a period of approximately 7–10 days in the stratosphere (Morris et al. 1995). The stratospheric polar vortex shift events toward the North Pacific (NP), North America (NA), and the Atlantic (ATL) are defined in the same way as EUR events. Based on this approach, we identify 45 EUR events, 23 NA events, and 30 ATL events for 1979–2015. There are no NP events according to our definition, which may be due to the Aleutian high over the North Pacific in the stratosphere, which inhibits a shift of the stratospheric polar vortex toward the North Pacific. We therefore focus on EUR, NA, and ATL events in the following analysis. In this study, the central date (see Table S1 in the supplemental material) of a vortex shift event is defined by the date of maximum fractional area coverage over the selected regions on the 850-K isentropic surface. In the following, the negative (positive) signs indicate days prior to (after) the central date unless otherwise stated.

Because of day-to-day variability in the polar vortex geometry, the polar vortex movement is partly related to its deformation. Therefore, following Seviour et al. (2013), we also calculate the aspect ratio of the polar vortex as a measure of its degree of stretching to analyze the influence of the polar vortex deformation on the polar vortex movement.

To analyze the tropospheric circulation prior to the polar vortex shift events, we calculate the frequency of tropospheric blocking events based on the tropospheric blocking index, which is calculated based on the equatorward and poleward meridional gradients of 500-hPa geopotential height fields (Davini et al. 2012, 2014):

$$\Delta_{\mathrm{eqw}} = \frac{\mathrm{Z500}(\lambda_0, \phi_0) - \mathrm{Z500}(\lambda_0, \phi_s)}{\phi_0 - \phi_S} \quad \text{and} \qquad (1)$$

$$\Delta_{\mathrm{plw}} = \frac{\mathrm{Z500}(\lambda_0, \phi_n) - \mathrm{Z500}(\lambda_0, \phi_0)}{\phi_n - \phi_0}, \qquad (2)$$

where λ_0 ranges from 0° to 360° in longitude, ϕ_0 ranges from 30° to 75°N, $\phi_s = \phi_0 - 15°$ latitude, and $\phi_n = \phi_0 + 15°$ latitude. The blocking index is defined with a value of 1 for days when the following conditions are fulfilled, and 0 otherwise:

$$\Delta_{\mathrm{eqw}} < 0 \text{ and } \Delta_{\mathrm{plw}} > -10 \text{ gpm } (^\circ \text{ lat})^{-1}. \qquad (3)$$

Considering that the blocking has sufficient spatial and temporal scales, as reported by Davini et al. (2014), we

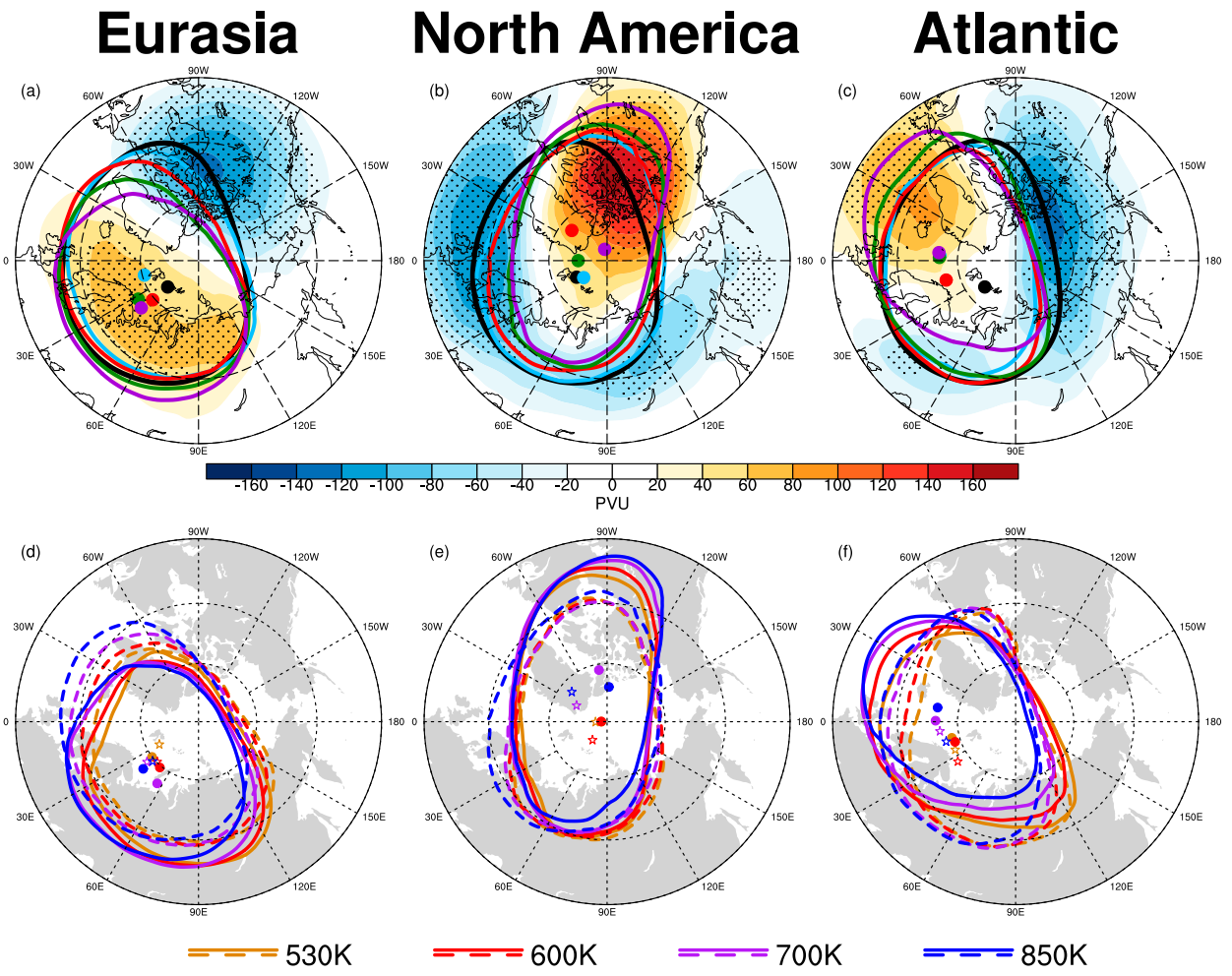

FIG. 1. (a) Anomalous PV fields (PVU;1 PVU $= 10^{-6}\,\mathrm{K\,kg^{-1}\,m^2\,s^{-1}}$; color shading) on the 850-K isentropic surface composited for 7 days before the central date of EUR events. Sky-blue, red, green, and purple contours (dots) represent the composite edge (center) of the stratospheric polar vortex on the 850-K isentropic surface at lag $= -7, -5, -3$, and -1 days, respectively. Black contour (dot) represents the composite daily climatological edge (center) of the stratospheric polar vortex on the 850-K isentropic surface for 7 days before the central date of EUR events. (b),(c) As in (a), but for NA and ATL events, respectively. (d) Composite distribution of stratospheric polar vortex edge and center on different isentropic surfaces (as shown in the legend) at lag $= -5$ days (edge: dashed lines; center: stars) and the central date (edge: solid lines; center: dots) of EUR events. (e),(f) As in (d), but for NA and ATL events, respectively. The anomalies over stippled regions are statistically significant with a 95% confidence level (based on the two-sided Student's t test).

apply the same spatial and temporal constraints to the aforementioned blocking index when defining a blocking event.

The two-sided Student's t test is employed to assess statistical significance in this study. The equivalent sample size is estimated using Eq. (4) in Zwiers and von Storch (1995). Following Wilks (2016), we use the false discovery rate (FDR) approach for multiple statistical tests to avoid overstatement of the results. The FDR algorithm operates on the collection of p values from multiple local significance tests and calculates a single global threshold for rejecting local null hypotheses when the local test is below the global threshold calculated based on Eq. (3) in Wilks (2016).

3. The characteristics of stratospheric polar vortex shift events

Figure 1 shows the evolution of the polar vortex edge and center for different stratospheric polar vortex shift events. For EUR events (Fig. 1a), as the lag time approaches the central date, the stratospheric polar vortex edge shifts as a whole toward Eurasia, accompanied by negative PV anomalies over North America and positive PV anomalies over Eurasia. The center of the stratospheric polar vortex also moves toward lower latitudes over Eurasia when the lag time approaches the central date. The pattern of the anomalous PV fields has a structure of a zonal wave 1. Previous studies also

indicated an amplification of zonal wave 1 during the stratospheric polar vortex shift events toward Eurasia (Castanheira and Barriopedro 2010; Zhang et al. 2016). As the central date of NA events (Fig. 1b) approaches, the stratospheric polar vortex begins to shift toward North America and away from Eurasia with statistically significant positive PV anomalies over North America. During NA events, the vortex shape is more elongated than that during EUR (Fig. 1a) and ATL events (Fig. 1c), and the vortex geometry is similar to that of the split SSWs reported in Matthewman et al. (2009). Note that the stratospheric polar vortex splits into two distinct vortices at lag = 0 days in their study, whereas the vortex shifts farther toward North America at lag = 0 days in the NA events. For ATL events (Fig. 1c), different segments of the polar vortex edge show inconsistent shifts. As time progresses, the segment of the polar vortex edge over the North Atlantic moves toward the equatorward side of its climatological segment with statistically significant positive PV anomalies over the North Atlantic.

The composite edges of the stratospheric polar vortex on different isentropic surfaces at lag = −5 days and the central date of EUR events tilt westward with altitude (Fig. 1d), while the composite stratospheric polar vortex shifts toward North America with altitude for NA events (Fig. 1e). For ATL events, the polar vortex edge shifts toward the North Atlantic with altitude (Fig. 1f). Although the tilts in the edge of the stratospheric polar vortex with altitude exist during EUR, NA, and ATL events, the stratospheric polar vortex shifts toward the three selected regions over time on the same isentropic surface. There are no systematic changes of the vortex center with altitude for EUR events; however, the stratospheric polar vortex centers on higher isentropic surfaces are mainly located in the Western Hemisphere for NA events, and the vortex center shifts toward the North Atlantic with altitude for ATL events.

As shown in Fig. 1, changes in the polar vortex geometry accompany the polar vortex shift. Thus, the influence of the polar vortex deformation on the movement of its position should be considered. According to the method of Seviour et al. (2013), we substitute the stratospheric polar vortex at 10 hPa (near the 850-K isentropic surface) with an equivalent ellipse and calculate the aspect ratio (AR) of the equivalent ellipse. Figure 2 shows the evolution of the composite AR (dashed line) and its climatology value (solid line) for different polar vortex shift events. The AR slowly decreases as the lag time approaches the central date of EUR events (Fig. 2a), but the difference between the composite AR and its climatology value is not statistically significant. For NA events (Fig. 2b), the AR gradually increases and reaches a maximum at lag = +3 days. The polar vortex also has a more elongated shape, as shown in Fig. 1b. The movement of the stratospheric polar vortex toward North America may be related to the stretching of the vortex. Before the central date of ATL events (Fig. 2c), the evolution of the AR fluctuates. The polar vortex shape also fluctuates, as shown in Fig. 1c.

Consider that the preconditioning of polar vortex shift events with different vortex deformations is likely different. In addition, the impact of the polar vortex shift events with different vortex deformations on the troposphere may be different, because the tropospheric circulation response to a polar vortex–induced PV anomaly depends on the shape of the polar vortex (Hoskins et al. 1985). Here, we divide the polar vortex shift events into those with small and large polar vortex deformation according to the polar vortex AR. A stratospheric polar vortex shift event is regarded as an event with small (large) polar vortex deformation when the number of days on which the absolute value of the difference between the daily AR and its climatology value is below (above) the 40th (60th) percentile of the absolute values of the differences for all selected events exceeding 6 days from lag = −10 days to the central date. As expected, the evolution of the composite AR of the stratospheric polar vortex shift events with small deformation (Figs. 2d–f) is more stable than that of the events with large deformation (Figs. 2g–i).

Figure 3 shows the evolution of the polar vortex edge and center for different stratospheric polar vortex shift events with small (Figs. 3a–c) and large (Figs. 3d–f) deformation. The geometry of the composite stratospheric polar vortex for EUR events with small deformation (Fig. 3a) is close to that of the climatological polar vortex. The stratospheric polar vortex as a whole shifts toward Eurasia, and the AR of the polar vortex is close to its climatology value (Fig. 2d). In addition, a persistent movement of the polar vortex center toward lower latitudes over the Eurasian continent can also be observed in Fig. 3a. The composite stratospheric polar vortex for EUR events with large deformation has a shape close to circular (Fig. 3d), which corresponds to a decrease in the AR (Fig. 2g). Compared to NA events with small deformation (Fig. 3b), the geometry of the stratospheric polar vortex is more elongated during NA events with large deformation (Fig. 3e). For ATL events with small deformation, the stratospheric polar vortex geometry is close to that of the climatological polar vortex (Fig. 3c), which is confirmed by the evolution of the AR (Fig. 2f). For ATL events with large deformation, the stratospheric polar vortex geometry

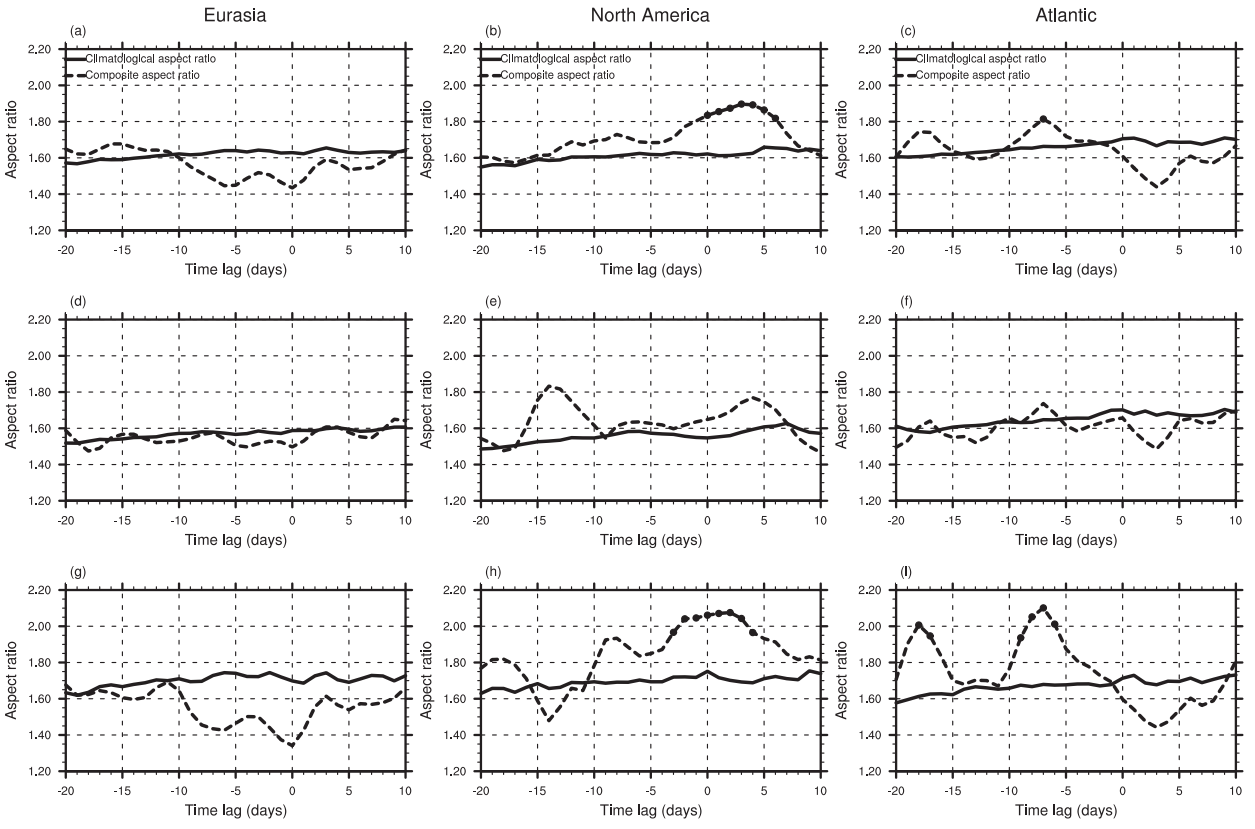

FIG. 2. (a) Composited daily AR time series of the stratospheric polar vortex (dashed line), which is calculated from 10-hPa geopotential height fields based on the method of Seviour et al. (2013), and its climatology value (solid line) for EUR events. (b),(c) As in (a), but for NA and ATL events, respectively. (d)–(f) As in (a)–(c), but for the events with small deformation. (g)–(i) As in (a)–(c), but for the events with large deformation. Dots along the dashed lines indicate that the composite AR is significantly different from its climatology value with a 95% confidence level (based on the two-sided Student's *t* test).

changes from elongated to approximately circular (Fig. 3f), which corresponds to a change from positive to negative anomalies in the AR (Fig. 2i).

4. The role of planetary waves in stratospheric polar vortex movements

Previous studies have indicated that planetary waves, especially zonal wave 1 and wave 2, play an important role in the variability of the stratospheric polar vortex (e.g., Polvani and Waugh 2004; Charlton and Polvani 2007; Martineau and Son 2013, 2015; Zhang et al. 2016; Huang et al. 2017; Li and Tian 2017). We therefore explore the variations in planetary waves and clarify the different precursors in the planetary wave patterns before the central date of stratospheric polar vortex shift events.

Figure 4 shows the latitude–pressure cross sections of the anomalous Eliassen–Palm (E-P) flux (vectors; Andrews and McIntyre 1976) and its divergence (contours) of zonal wave 1 (Figs. 4a–c) and wave 2 (Figs. 4d–f) for the three types of polar vortex shift events averaged from lag = −7 to −1 days. We choose this period to focus on the main characteristics of the zonal wave-1 and wave-2 activity in earlier stages of stratospheric polar vortex shift events.

For EUR events, there are anomalous upward zonal wave-1 E-P fluxes from 50° to 70°N in the troposphere (Fig. 4a) before the central date. The anomalous zonal wave-1 E-P fluxes near the tropopause are directed equatorward and upward (Fig. 4a). The anomalous upward wave-1 E-P fluxes enter the stratosphere and lead to anomalous convergence of the E-P flux (Fig. 4a) in the polar stratosphere. The structure of the anomalous zonal wave-1 E-P flux is similar to that in the prewarming phase of SSWs reported by Limpasuvan et al. (2004). Previous studies also indicated an enhanced zonal wave 1 in the stratosphere prior to the displacement SSWs (Charlton and Polvani 2007; Martius et al. 2009; Castanheira and Barriopedro 2010). Note, however, that the centers of zonal wave-1 geopotential height anomalies at 10 hPa (~850 K) are along an axis

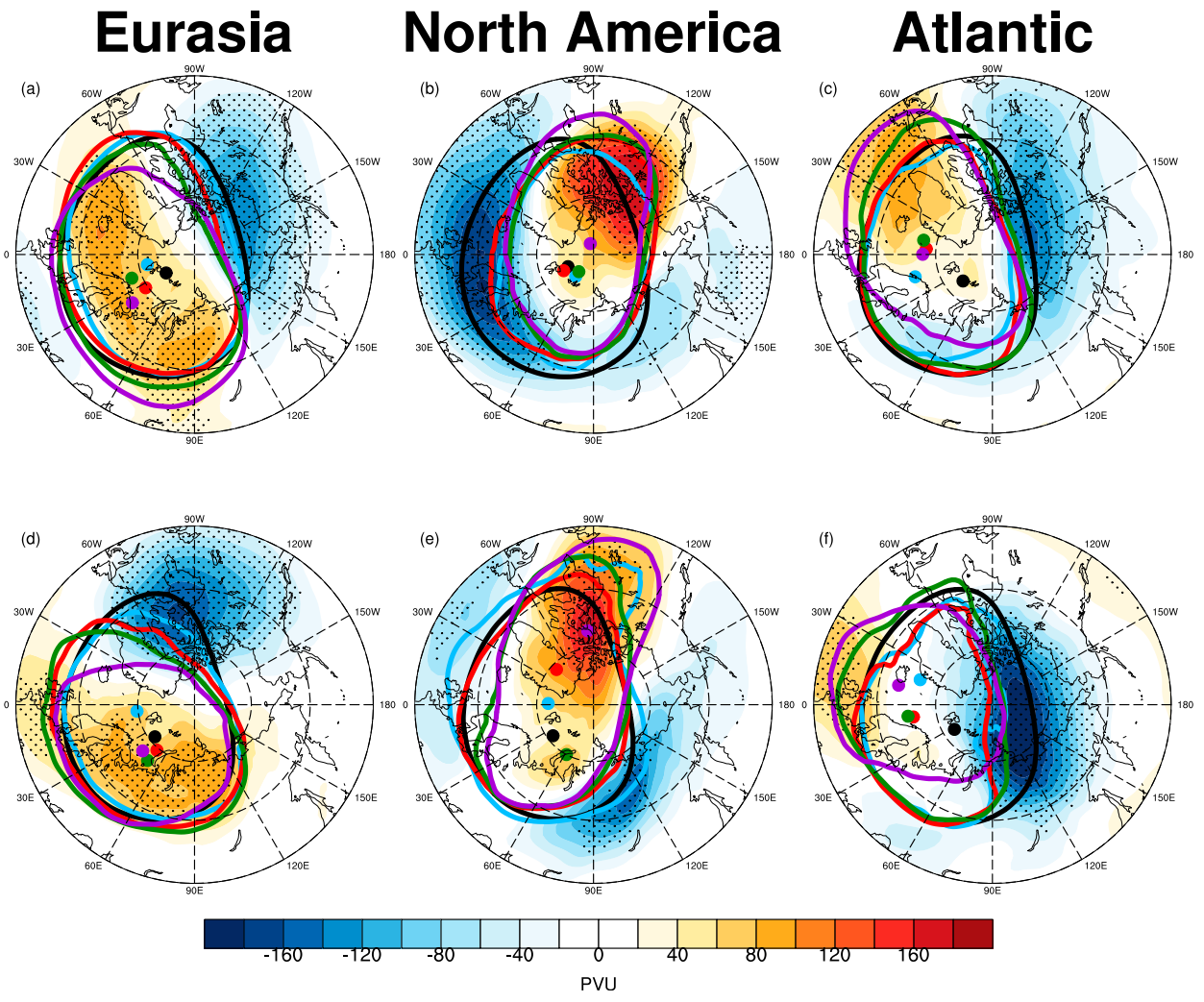

FIG. 3. As in Fig. 1, but for stratospheric polar vortex shift events with (a)–(c) small polar vortex deformation and the events with (d)–(f) large polar vortex deformation.

approximately parallel to the 30°E–150°W circle in the study of Martius et al. (2009), whereas the centers are along an axis almost parallel to the 60°E–120°W circle in our study (Figs. S1a–d in the supplemental material). The anomalous zonal wave-2 E-P fluxes indicate a weaker-than-average wave activity entering the stratosphere (Fig. 4d).

For NA events, the zonal wave-1 E-P fluxes entering the stratosphere are anomalously weak before the central date (Fig. 4b), and the reduced upward E-P fluxes lead to anomalous wave-1 E-P flux divergence. The structure of zonal wave-2 E-P fluxes (Fig. 4e) is almost opposite to that of zonal wave-1 E-P fluxes. Anomalous upward wave-2 E-P fluxes are entering the stratosphere, and anomalous convergence is occurring in the polar stratosphere. Although zonal wave 1 is weakened before NA events, we note that the patterns of zonal wave-1 (Figs. S1e–h) and wave-2 (Figs. S2e–h) geopotential height anomalies at 10 hPa, both of which have negative centers over North America, are together responsible for shifting the stratospheric polar vortex toward North America.

The composites of ATL events also show enhanced zonal wave-1 E-P fluxes entering the stratosphere before the central date (Fig. 4c). The zonal wave-2 E-P fluxes (Fig. 4f) entering the stratosphere are anomalously weak, as are those in EUR events. Although both EUR and ATL events show an enhanced zonal wave 1 and a weakened zonal wave 2 in the stratosphere, the patterns of zonal wave-1 (Figs. S1i–l) and wave-2 (Figs. S2i–l) geopotential height anomalies are different during the two types of events. The orientation of the wave-1 activity during ATL events is more closely centered over the Atlantic.

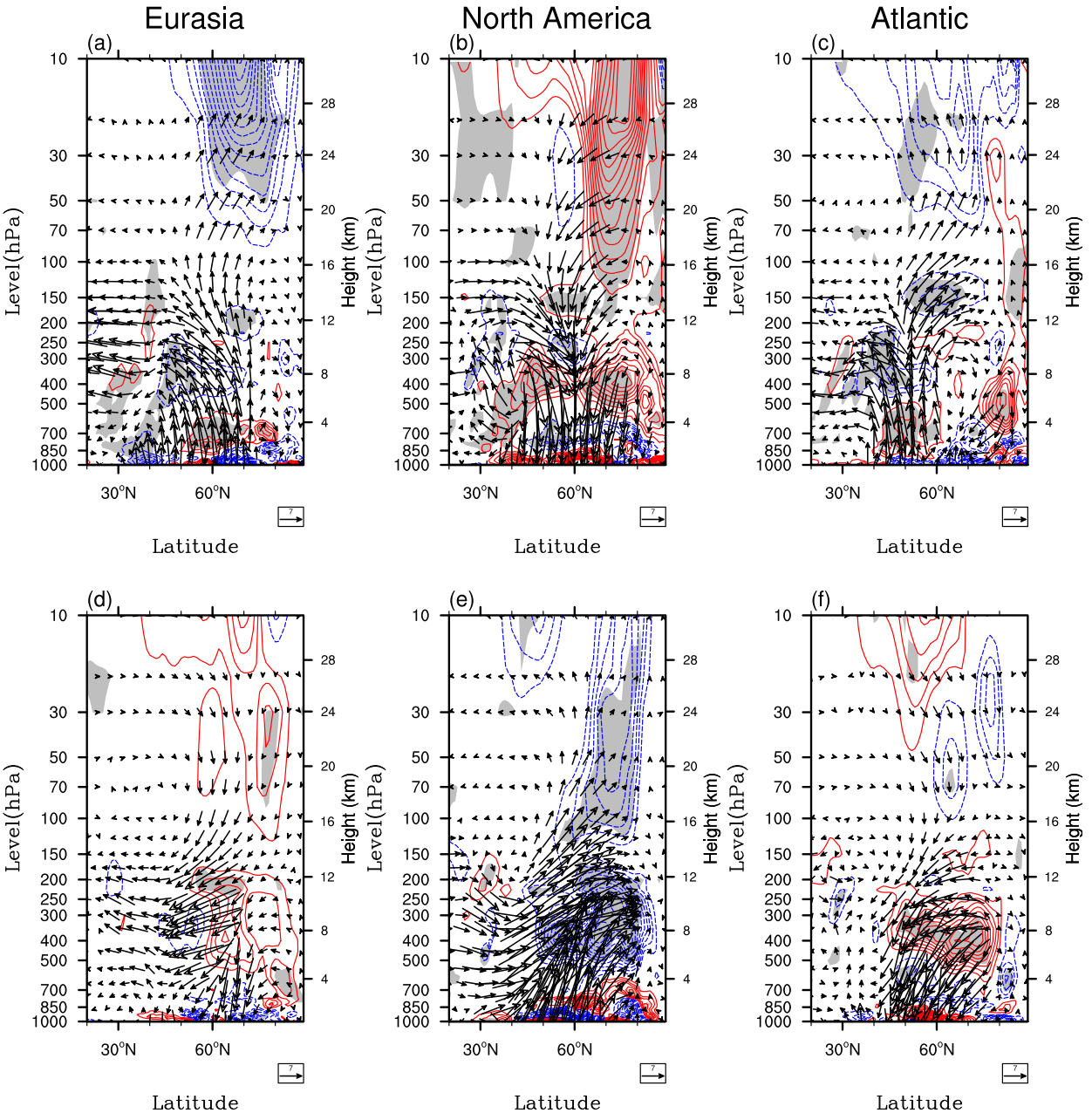

FIG. 4. (a) Latitude–pressure cross sections of anomalous E-P flux (vectors) and its divergence (contours) of zonal wave 1 for EUR events. The meridional and vertical components of the E-P flux are divided by 10^6 and 10^4 before the composites, respectively. The reference vector lengths of the E-P flux are 7 kg s^{-2}. The contour interval for the divergence of the E-P flux is 0.5 m s^{-1} day^{-1}. Blue dashed and red solid lines represent negative and positive values, respectively, and zero contours are omitted. (b),(c) As in (a), but for NA events and ATL events, respectively. (d)–(f) As in (a)–(c), but for zonal wave 2. Areas with gray shading are statistically significant with a 95% confidence level (based on the two-sided Student's *t* test).

The zonal wave-1 and wave-2 behaviors for different stratospheric polar vortex shift events are further highlighted in Fig. 5. Figure 5 shows composites of the daily anomalies of the meridional heat flux of zonal wave 1 (blue lines) and wave 2 (red lines) at 100 hPa, area-averaged between 45° and 75°N. EUR events are preceded by enhanced zonal wave-1 activity entering the lower stratosphere within 7 days before the central date (Fig. 5a). The negative anomalies of the zonal wave-2 heat flux within 10 days before the central date indicate weak zonal wave-2 activity entering the lower stratosphere (Fig. 5a). The evolution of heat flux anomalies

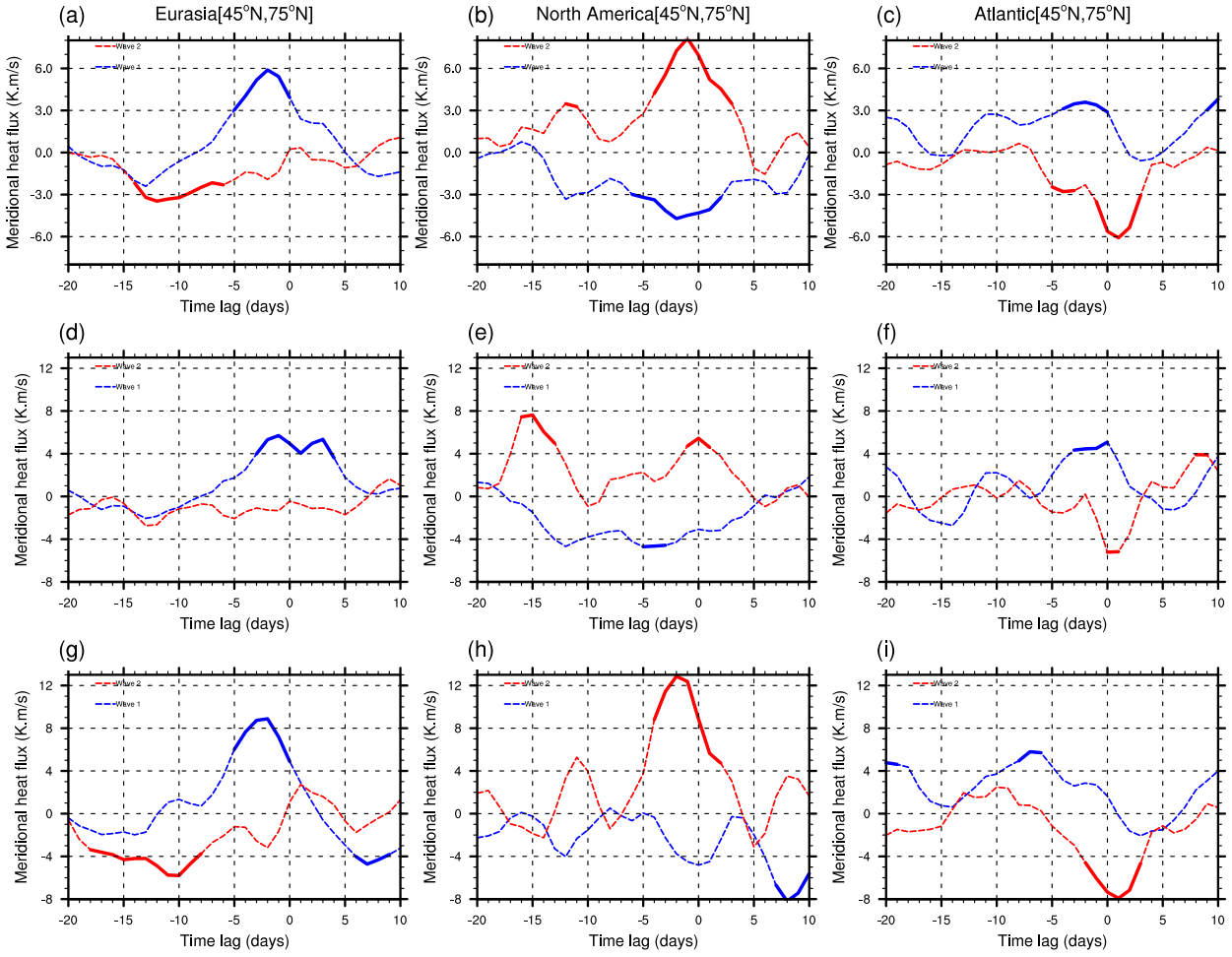

FIG. 5. (a) Composites of daily anomalies of zonal wave-1 (blue dashed lines) and wave-2 (red dashed lines) meridional heat flux (K m s^{-1}) at 10 hPa averaged between 45° and 75°N for EUR events. (b),(c) As in (a), but for NA events and ATL events, respectively. (d)–(f) As in (a)–(c), but for events with small deformation. (g)–(i) As in (a)–(c), but for events with large deformation. Day zero refers to the central date. Thick line segments indicate anomalies significantly different from zero at the 95% confidence level (based on the two-sided Student's *t* test).

before the central date is similar to that of displacement SSWs (Charlton and Polvani 2007) and that of wave-1 SSWs (Bancalá et al. 2012), except for the shorter persistence of positive zonal wave-1 heat flux anomalies in our study, which may be related to some non-SSWs included in our study (as shown in Table S1).

The composites of NA events show a characteristic (Fig. 5b) that is almost opposite to that of EUR events (Fig. 5a). The composite anomalous heat fluxes show enhanced zonal wave-2 activity and weakened zonal wave-1 activity entering the lower stratosphere within five days before the central date. This is in contrast to previous studies that concentrated only on events that eventually led to the total breakdown (as split SSWs) that show positive zonal wave-2 energy anomalies preceded by positive zonal wave-1 energy anomalies, before the central date of split SSWs (Martius et al. 2009; Castanheira and Barriopedro 2010). The reduced wave energy entering the lower stratosphere in our selection of events is likely because the selected events do not result in a split polar vortex.

For ATL events, the composites of the anomalous heat flux show enhanced zonal wave-1 activity and weakened zonal wave-2 activity entering the lower stratosphere (Fig. 5c). The anomalous zonal wave-1 heat fluxes before the central date of ATL events are weaker than those of EUR events.

We now examine the similarities and differences of planetary wave precursor activity between the events with large vortex deformation and those with small vortex deformation. Before the central date of EUR events, enhanced zonal wave-1 activity into the lower

stratosphere occurs with both small- and large-deformation events (Figs. 5d and 5g, respectively). The zonal wave-2 heat flux anomalies for EUR events with small deformation are small and statistically insignificant (Fig. 5d), but relatively large and statistically significant negative zonal wave-2 heat flux anomalies occur before the central date of EUR events with large deformation (Fig. 5g). The decrease in zonal wave-2 activity entering the stratosphere may weaken the elongation of the stratospheric polar vortex and then lead to an approximately circular polar vortex relative to its climatological counterpart (Fig. 3d).

Enhanced zonal wave-2 activity into the lower stratosphere is evident prior to NA events with both small and large deformation (Figs. 5e and 5h, respectively). An evident difference is that the amplitude of the positive zonal wave-2 heat flux anomalies prior to the central date of NA events with large deformation is larger than that of the small-deformation events. Therefore, the stratospheric polar vortex in NA events with large deformation is more elongated (Fig. 3e) than that in the small-deformation events because of the higher amounts of zonal wave-2 activity entering the stratosphere.

Zonal wave-1 activity into the lower stratosphere prior to ATL events is enhanced with both small and large deformation (Figs. 5f and 5i, respectively). However, zonal wave-2 heat flux anomalies change from positive to negative during ATL events with large deformation (Fig. 5i). This corresponds to a change of the AR from larger to smaller than its climatology value (Fig. 2i), and the stratospheric polar vortex geometry changes from an elongated shape to an approximately circular shape (Fig. 3f). Thus, the zonal wave 2 entering the stratosphere plays an important role in the change in stratospheric polar vortex geometry.

5. The links between the polar vortex shift events and the tropospheric weather patterns

Previous studies have indicated that the variability in the troposphere can impact the stratospheric polar vortex (e.g., Polvani and Waugh 2004), as discussed in section 1. The impacts of Arctic sea ice, Eurasian snow cover, and El Niño–Southern Oscillation (ENSO) on the stratospheric polar vortex are evident over relatively longer time scales, whereas the influence of tropospheric blocking on the stratospheric polar vortex, which is the only impact discussed in this study, is important over relatively shorter time scales. In this section, we examine the connections between the spatial patterns of zonal wave-1 and wave-2 geopotential height anomalies and the patterns of tropospheric blocking before the central date of different stratospheric polar vortex shift events.

Figure 6 shows the composite anomalous blocking frequency averaged from lag = −7 to −1 days for all stratospheric polar vortex shift events (Figs. 6a–c), events with small deformation (Figs. 6d–f), and events with large deformation (Figs. 6g–i). For EUR events, the main characteristics of the pattern of anomalous tropospheric blocking before the central date include statistically significant positive blocking frequency anomalies over northern Europe and the Ural Mountains and negative blocking frequency anomalies over the Bering Strait and parts of the Far East (Fig. 6a). The blocking frequency anomalies detected south of 40°N are not included in the subsequent analysis because of their negligible impact on the midlatitude circulation (Davini et al. 2012). Previous studies have noted that the anomalous blocking patterns described above can lead to enhanced zonal wave-1 activity and weakened zonal wave-2 activity entering the lower stratosphere, respectively (Martius et al. 2009; Castanheira and Barriopedro 2010; Woollings et al. 2010; Nishii et al. 2011; Huang et al. 2017). A clear depiction of how tropospheric blocking might influence the planetary-scale wave activity in the stratosphere is shown in Fig. 7, which shows the composite of the zonal wave-1 and wave-2 geopotential height anomalies and the zonal wave-1 and wave-2 Plumb flux (Plumb 1985) anomalies along 60°N. As shown in Fig. 7a, the anomalous zonal wave 1 shifts westward with altitude and has a negative center (indicated by a white line) over Eurasia in the middle and lower stratosphere. This feature is consistent with the westward shift of the stratospheric polar vortex with altitude (Fig. 1d). This implies that the polar vortex might not cover Eurasia in the upper stratosphere; however, the position of the polar vortex in the middle and lower stratosphere has a larger impact on the troposphere than that in the upper stratosphere. Therefore, polar vortex shifts occurring in the middle and lower stratosphere only are discussed in this study. The anomalous Plumb fluxes indicate that the zonal wave-1 component of the Plumb fluxes is anomalously directed upward. The anomalous zonal wave 2 shows no shift with altitude and is weakened because of the out-of-phase superposition with its climatological wave 2 (Fig. 7d).

There are positive blocking frequency anomalies over the Bering Strait and parts of the Far East and negative blocking frequency anomalies over northern Europe before the central date of NA events (Fig. 6b). A comparison between the patterns of tropospheric blocking prior to split SSWs and prior to NA events shows that both types of events have positive blocking frequency

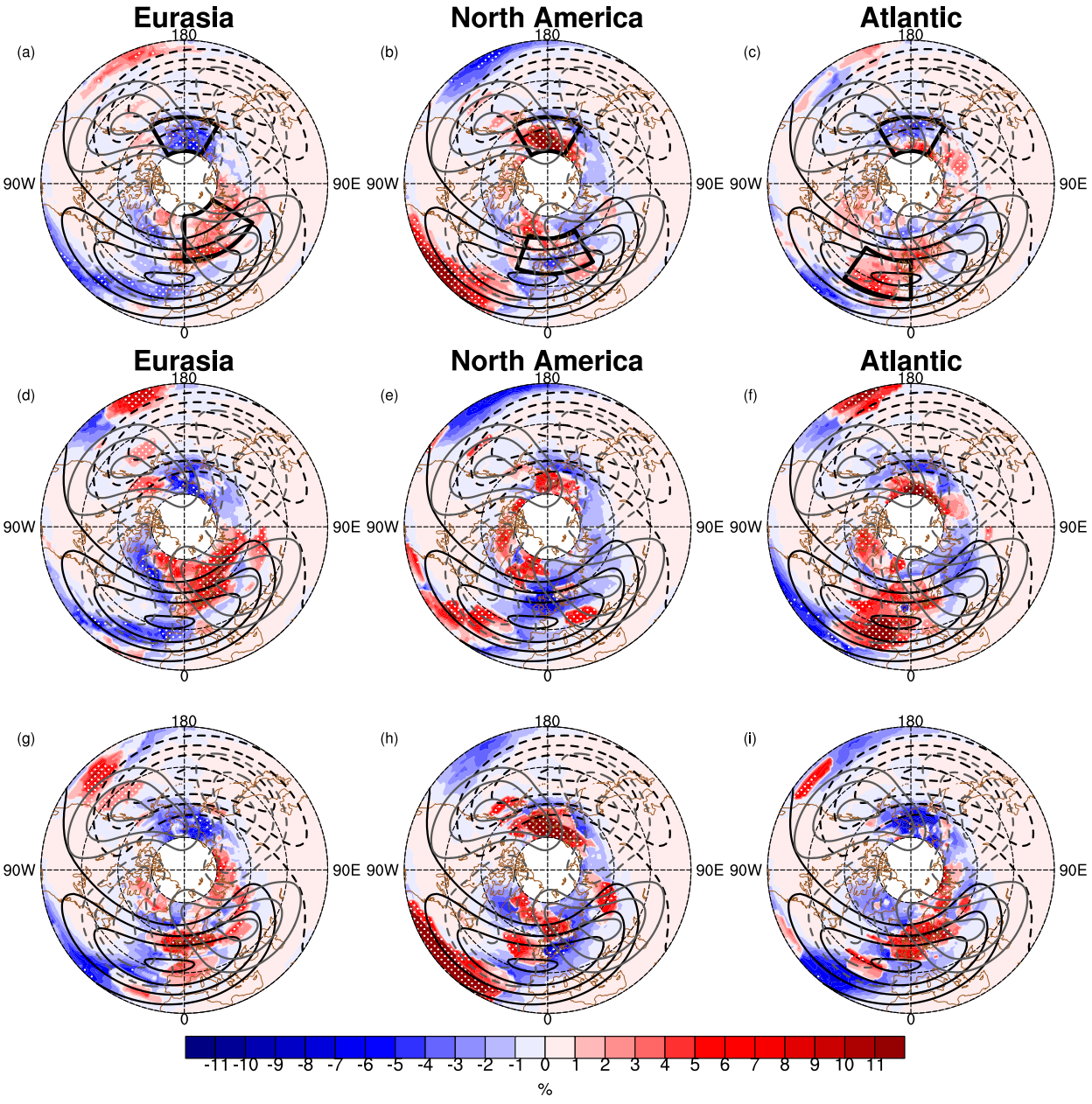

FIG. 6. (a) Composite anomalous blocking frequency (color shading, with interval of 1%) and climatological zonal wave 1 (black contours, with interval of 25 gpm) and zonal wave 2 (gray contours, with interval of 25 gpm) in winter at 500 hPa for EUR events. (b),(c) As in (a), but for NA and ATL events, respectively. (d)–(f) As in (a)–(c), but for the events with small deformation. (g)–(i) As in (a)–(c), but for the events with large deformation. The anomalies over stippled regions are statistically significant with a 90% confidence level (based on the two-sided Student's *t* test). Boxes represent the domains over which the area-weighted blocking frequency anomalies are computed.

anomalies over the Bering Strait and that increased blocking days exist over northern Europe during split SSWs (Nishii et al. 2011) but not during NA events. In Fig. 7b, we can observe that the anomalous zonal wave 1 shifts westward with altitude and has a negative center over North America in the middle and lower stratosphere. In addition, the anomalous zonal wave 2 has one of its negative centers over North America (Fig. 7e).

During ATL events, positive blocking frequency anomalies occur over the eastern North Atlantic and parts of Europe, and negative blocking frequency anomalies exist over the Bering Strait and parts of the Far East (Fig. 6c). Interestingly, the anomalous blocking frequency pattern during ATL events is similar to that during EUR events (Fig. 6a). However, there are also differences in these two blocking frequency patterns.

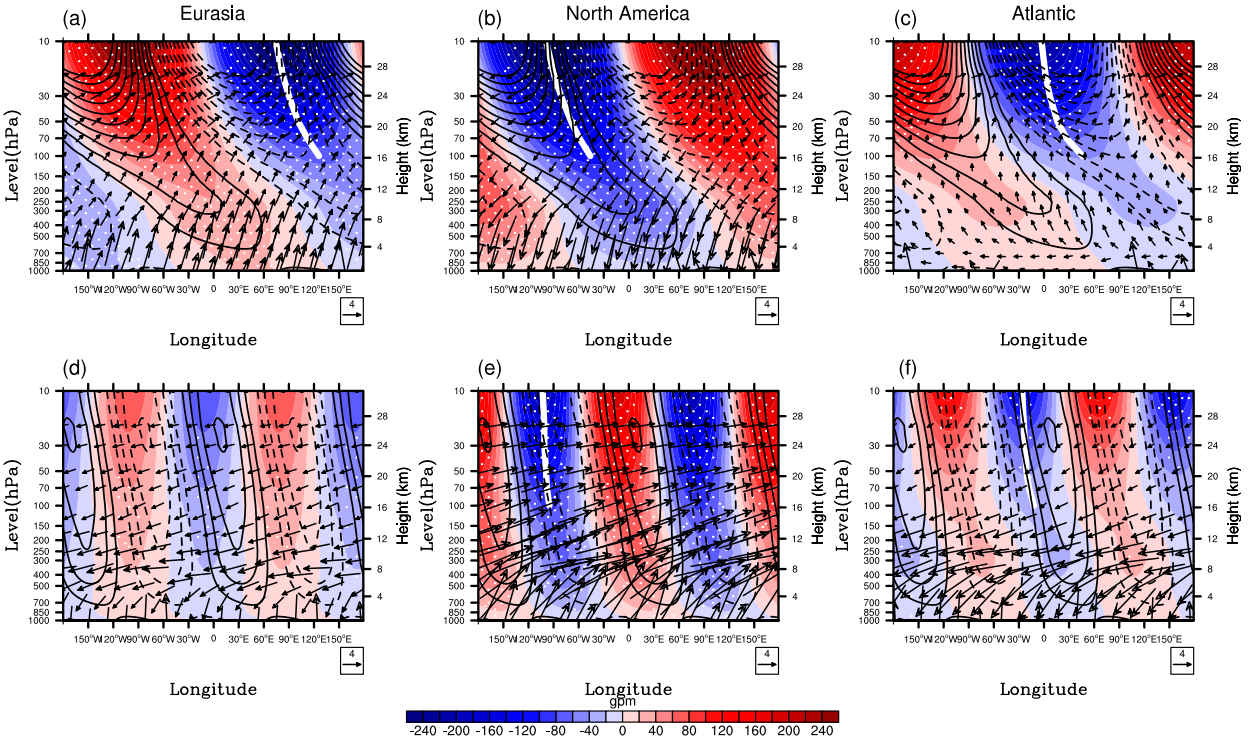

FIG. 7. (a) Longitude–pressure cross sections of the composite of zonal wave-1 geopotential height anomalies (color shading, with interval of 20 gpm) and zonal wave-1 Plumb flux anomalies (vectors) along 60°N for EUR events. The reference vector lengths of the Plumb flux are 4 m^2 s^{-2}. Solid (dashed) contours represent positive (negative) values of the climatology of zonal wave-1 geopotential height anomalies along 60°N for the period 1979–2015. The contour interval is 40 gpm, and zero contours are omitted. (b),(c) As in (a), but for NA and ATL events, respectively. (d)–(f) As in (a)–(c), but for zonal wave 2. White lines indicate the negative center of planetary waves in the stratosphere. The anomalies over stippled regions are statistically significant with a 95% confidence level (based on the two-sided Student's *t* test).

The amplitudes of both the positive and the negative anomalies in the blocking frequency during ATL events are smaller than those during EUR events. In addition, statistically significant positive blocking frequency anomalies exist over the eastern Atlantic, which is the positive center of climatological wave 1 (contours in Fig. 6c) at 500 hPa, during ATL events but not during EUR events (Fig. 6a). Thus, the phase difference between the anomalous zonal wave 1 and its climatological wave 1 for ATL events (Fig. 6c) is less than that for EUR events (Fig. 7a). Both the anomalous zonal wave 1 and wave 2 have negative centers over the Atlantic in the middle and lower stratosphere (Figs. 7c and 7f, respectively).

We also examine the similarities and differences of the spatial patterns of tropospheric blocking frequency anomalies between the vortex shift events with small and large deformation. Both types of EUR events have negative blocking frequency anomalies over the Bering Strait (Figs. 6d,g). The positive blocking frequency anomalies are located in northern Europe prior to EUR events with small deformation and in western Europe prior to EUR events with large deformation. There are negative blocking frequency anomalies over northern Europe for both types of NA events (Figs. 6e,h). The amplitude of the positive blocking frequency anomalies during NA events with large deformation (Fig. 6h) is larger than that during NA events with small deformation (Fig. 6e). This is consistent with a more evident zonal wave-2 heat flux in NA events with large deformation (Fig. 5h). An apparent difference between ATL events with small and large deformation is that the positive blocking frequency anomalies exist the eastern Atlantic, where the center of climatological zonal wave 1 (Fig. 6f) at 500 hPa is located, during ATL events with small deformation but that these anomalies shift northward in ATL events with large deformation (Fig. 6i). Therefore, the polar vortex in ATL events with small deformation shows a persistent shift toward the Atlantic (Fig. 3c).

Based on previous analysis, one might expect a bidirectional statistical link between stratospheric polar vortex shift events and tropospheric blocking. It has been shown that by identifying the stratospheric polar vortex shift events toward different regions, one can obtain different patterns of tropospheric blocking

frequency anomalies. Similarly, we define three types of the most evident tropospheric blocking events that have a similar spatial pattern of blocking frequency anomalies as the patterns prior to EUR, NA, and ATL events and verify whether these patterns match the stratospheric polar vortex movement toward the three selected regions. We take the tropospheric events that match the blocking patterns of EUR events (EUR blocking events) as an example. We calculate the daily difference between the area-weighted blocking frequency anomalies over northern Europe and the Bering Strait during winter from 1979 to 2015. These two selected domains (boxes in Fig. 6a) correspond well to the regions of the positive and the negative blocking frequency anomalies in the blocking patterns before EUR events. Then, the difference defined above is ranked, and once an event is selected, the subsequent 15 days are eliminated. This separation ensures sufficient time for separating the two adjacent blocking events. The top 40 events are retained for analysis. For tropospheric events matching the blocking patterns of NA events (NA blocking events), the Bering Strait and northern Europe (boxes in Fig. 6b) are chosen to calculate the blocking frequency difference. For tropospheric events matching the blocking patterns of ATL events (ATL blocking events), the difference between the blocking frequency over the eastern Atlantic and that over the Bering Strait (boxes in Fig. 6c) is calculated.

Figure 8a shows the composite stratospheric polar vortex edge and center on the 850-K isentropic surface at various lag times relative to the peak blocking frequency difference for EUR blocking events. Note that the lag time should not be compared among previous figures, since the central date of the stratospheric polar vortex shift events might not match the peak value in the blocking frequency differences. The stratospheric polar vortex shows a persistent shift toward Eurasia. In addition, the polar vortex center is also shifted toward lower latitudes, and statistically significant positive PV anomalies exist over central Eurasia. For NA blocking events, the stratospheric polar vortex is also displaced toward North America with only small deformation, and the polar vortex center moves toward North America over time (Fig. 8b). Although there is no evident shift of the stratospheric polar vortex edge toward the Atlantic for ATL blocking events, the polar vortex center shows a consistent shift toward the Atlantic (Fig. 8c).

In addition, we compare the likelihood of the stratospheric polar vortex shift toward one of the three selected regions in the presence and absence of the EUR, NA, and ATL blocking patterns. Figures 8d–f show the stratospheric polar vortex edges and centers under the condition of all the blocking events with and without the defined blocking patterns at lag = 0 (red), 2 (green), and 4 (purple) days relative to the day with the peak blocking frequency difference. It is found that the stratospheric polar vortex overall prefers to shift toward Eurasia, North America, and the Atlantic when the tropospheric blocking patterns detected in our analysis exist prior to EUR, NA, and ATL events, respectively. Furthermore, we quantify the likelihood of the polar vortex shift toward Eurasia, North America, and the Atlantic during a 10-day period in the presence of defined EUR, NA, and ATL blocking events, respectively. Our reanalysis reveals the likelihood of the polar vortex shift toward Eurasia is 26.5% following the blocking events without EUR blocking patterns, whereas the likelihood is increased to 47.3% following EUR blocking events (a 20.8% increase). There is a 13.3% chance of the polar vortex shift toward North America following the blocking events without NA blocking patterns and a 22.7% chance following NA blocking events (a 9.4% increase). The likelihood of the polar vortex shift toward the Atlantic increases from 10.5% without ATL blocking patterns to 14.8% following ATL blocking events (a 4.3% increase).

Different stratospheric polar vortex shift events can exert different impacts on the troposphere. As shown in Fig. 9, the three types of stratospheric polar vortex shifts lead to PV increases in the lower stratosphere over Asia, North America, and the Euro–Atlantic region. Hoskins et al. (1985) pointed out that the tropopause tends to bow toward the troposphere in response to a positive PV anomaly in the lower stratosphere. Thus, there are statistically significant negative height anomalies at 250 hPa over northern Eurasia (Fig. 9a), North America (Fig. 9b), and the northern Atlantic (Fig. 9c) during EUR, NA, and ATL events in response to PV increases in the lower stratosphere over these regions, respectively.

It should be pointed out that there exist differences in the circulation responses near the tropopause to the polar vortex shift events with small and large deformation. The geopotential height anomalies over the North Pacific are positive during EUR events with small deformation but negative during EUR events with large deformation. The difference in the spatial pattern of height anomalies is closely related to the difference in the spatial pattern of PV anomalies in the lower stratosphere, with positive PV anomalies during large-deformation events (Fig. 9g) and negative PV anomalies in small-deformation events (Fig. 9d). An evident difference between the two types of NA events is that the amplitude of negative height anomalies over North America during large-deformation NA events (Fig. 9h) is larger than that during small-deformation NA events

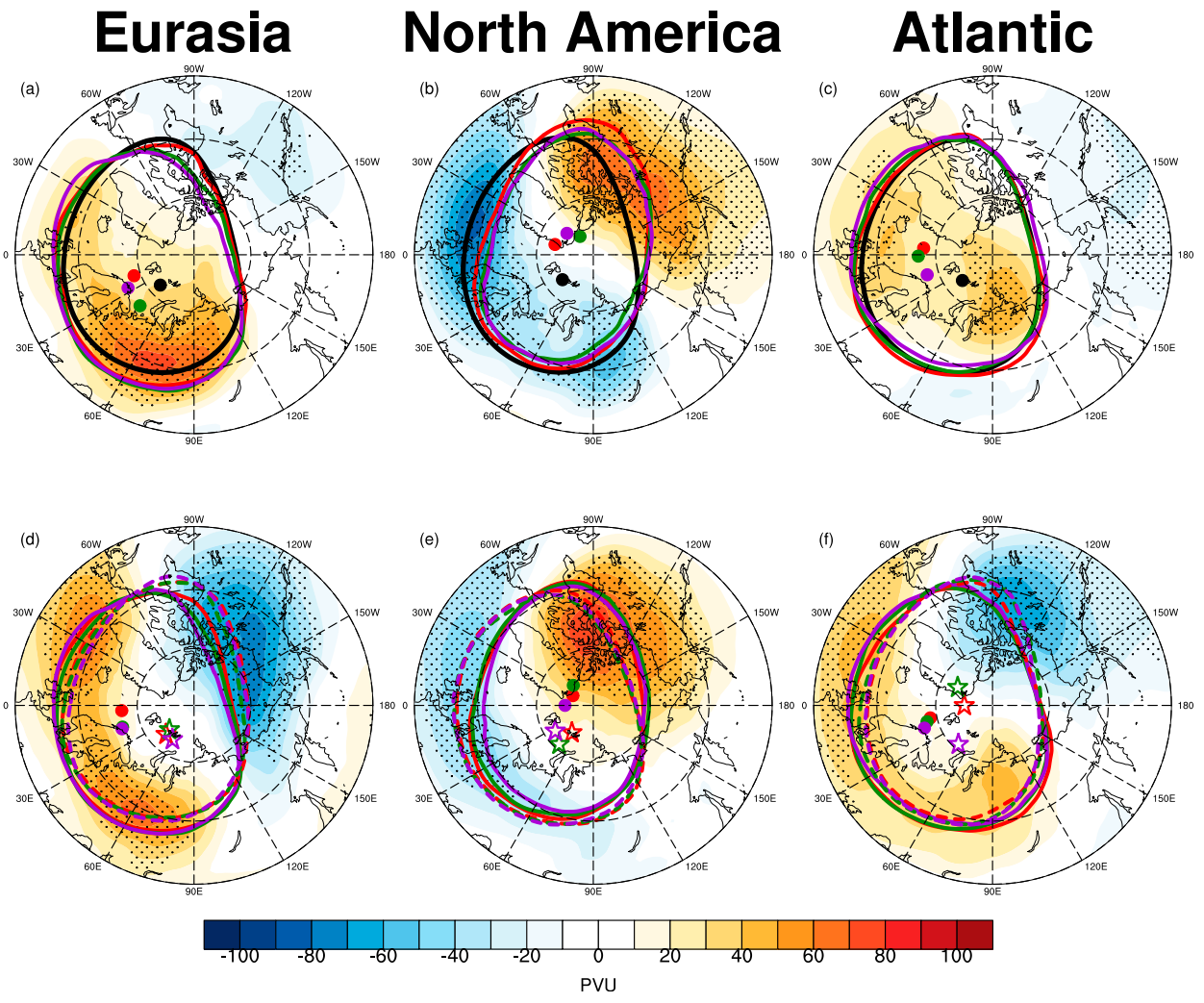

FIG. 8. (a) Anomalous PV fields (PVU; color shading) on the 850-K isentropic surface composited from lag = −6 to 6 days relative to the central date of EUR blocking events. (b),(c) As in (a), but for NA and ATL blocking events, respectively. (d)–(f) As in (a)–(c), but for the difference of the anomalous PV fields for all the blocking events with and without the defined blocking patterns as those in the EUR, NA, and ATL events, respectively. Black contour (dot) represents the composite daily climatological edge (center) of the stratospheric polar vortex on the 850-K isentropic surface. Solid contours (dots) represent the composite edge (center) of the stratospheric polar vortex on the 850-K isentropic surface at lag = 0 (red), 2 (green), and 4 (purple) days for the blocking events with the defined blocking patterns. Dashed contours (stars) represent the composite edge (center) of the stratospheric polar vortex for the blocking events without the defined blocking patterns. Stippling indicates that the anomalies are statistically significant with a 95% confidence level (based on the two-sided Student's *t* test). See text for the details of the definition of EUR, NA, and ATL blocking events.

(Fig. 9e). This is mainly related to larger PV anomalies over North America in large-deformation events than those in small-deformation events. The pattern of height anomalies in ATL events with small deformation (Fig. 9f) is similar to that in all ATL events, but the height anomalies during ATL with large deformation are statistically insignificant.

To provide more insight into the impacts of polar vortex shifts on the Northern Hemisphere surface climate, only those events in which the area-weighted PV anomalies (boxes in Fig. 9) extend from the 850-K isentropic surface down to the 300-K isentropic surface are selected for analysis. Figure 10 shows surface air temperature (SAT) anomalies for the period from −4 to 4 days relative to the day with the maximum value of area-weighted PV anomalies during EUR, NA, and ATL events (Figs. 10a–c). The corresponding results during these three types of events with small vortex deformation (Figs. 10d–f) and events with large vortex deformation (Figs. 10g–i) are shown for comparison. Statistically significant surface cooling anomalies over northern Eurasia in EUR events are likely related to the

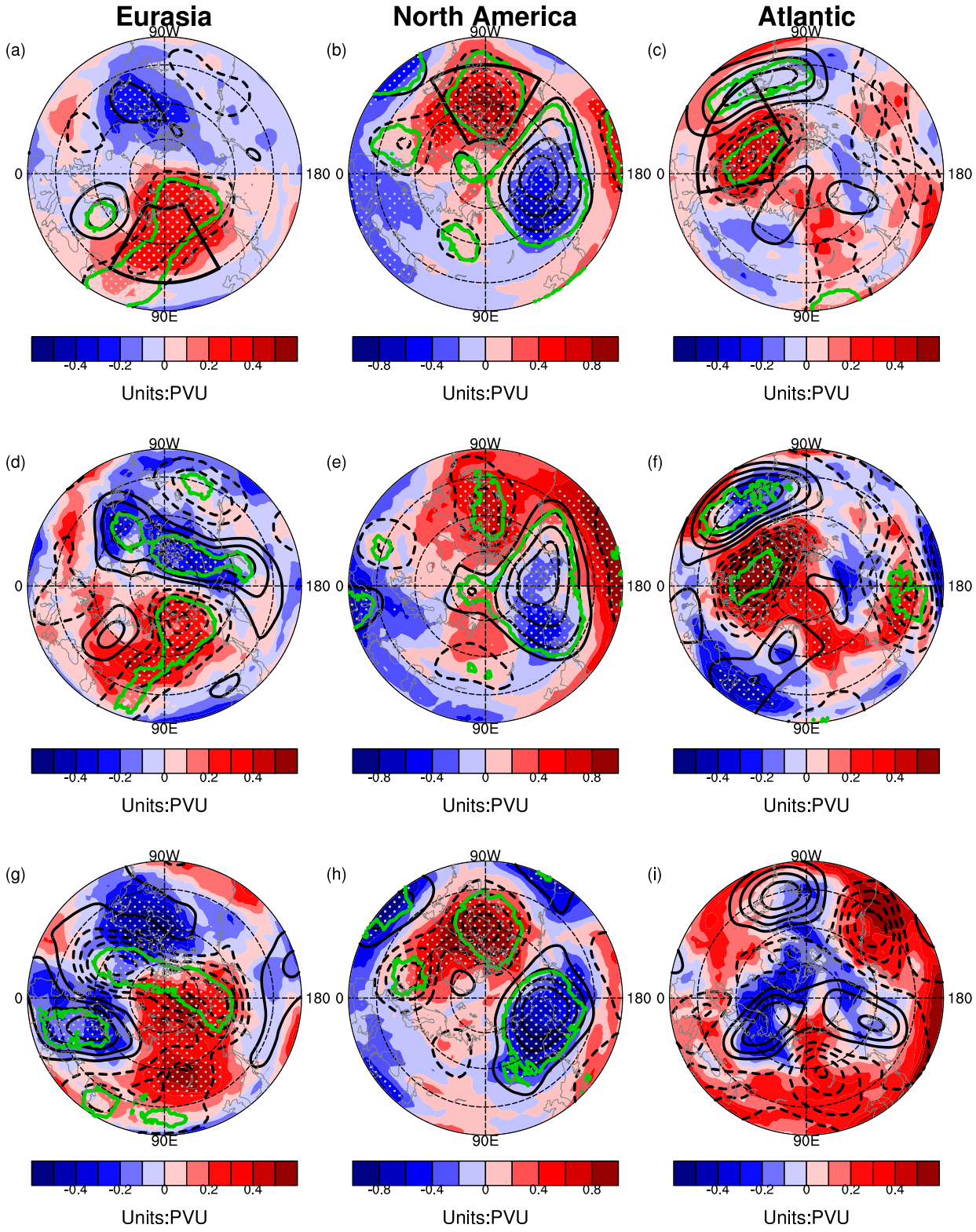

FIG. 9. (a) The composite geopotential height anomalies at 250 hPa (contours) and PV anomalies on the 370-K isentropic surface (shading) for the period from −4 to 4 days relative to the day with a maximum value of area-averaged (boxes) PV anomalies in the lower stratosphere (vertically averaged from the 330- to the 430-K isentropic surface) for EUR events. (b),(c) As in (a), but for NA and ATL events, respectively. (d)–(f) As in (a)–(c), but for events with small deformation. (g)–(i) As in (a)–(c), but for events with large deformation. The contour interval is 20 gpm for EUR and ATL events and 40 gpm for NA events, and zero contours are omitted, with positive in solid and negative in dashed. Stippling (green contour) indicates that the PV (geopotential height) anomalies are statistically significant with a 95% confidence level (based on the two-sided Student's *t* test).

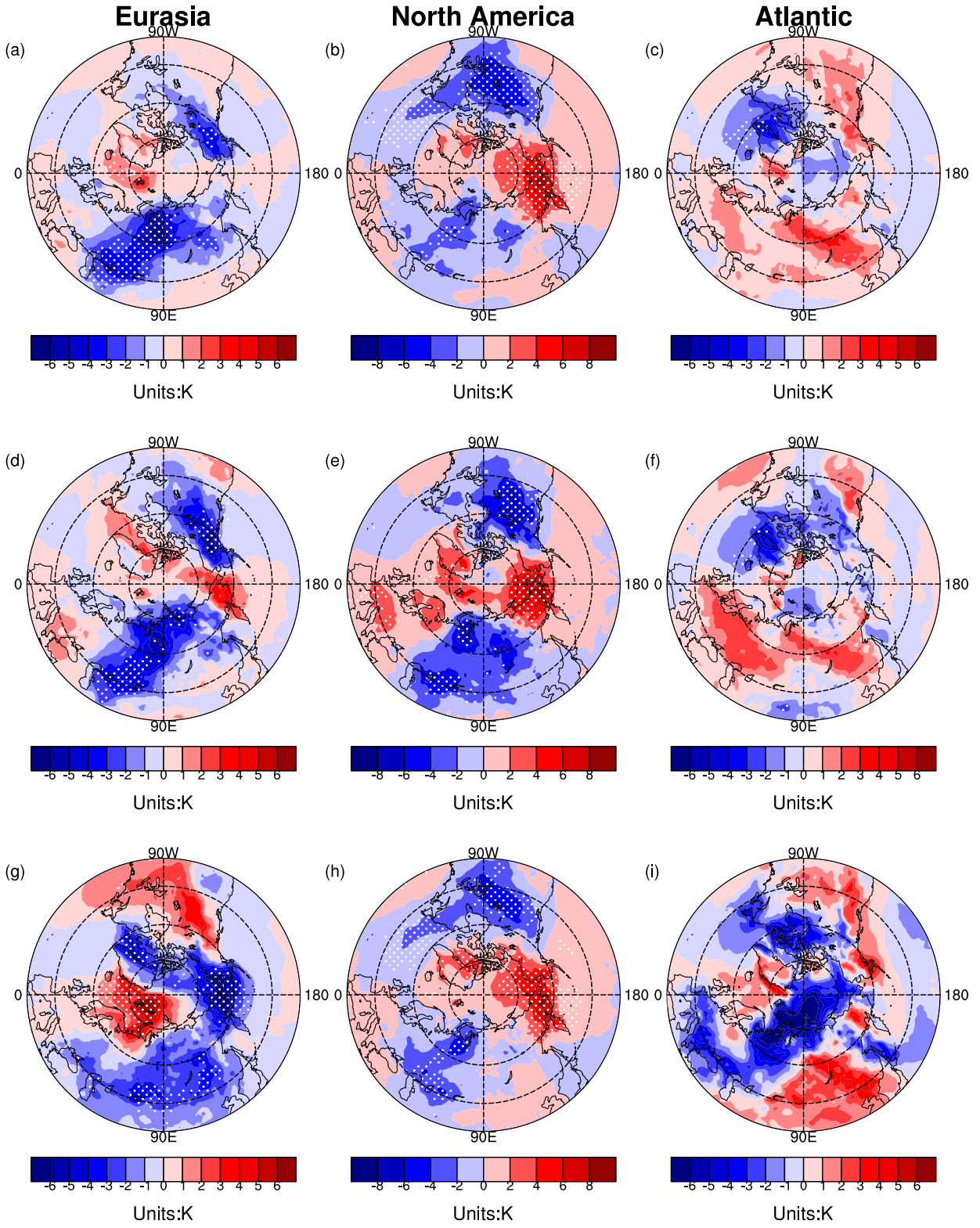

FIG. 10. (a) The composite SAT anomalies for the period from −4 to 4 days relative to the day with a maximum value of area-averaged PV anomalies during EUR events. (b),(c) As in (a), but for NA and ATL events, respectively. (d)–(f) As in (a)–(c), but for events with small deformation. (g)–(i) As in (a)–(c), but for events with large deformation. The anomalies over stippled regions are statistically significant with a 95% confidence level (based on the two-sided Student's *t* test).

shift of the polar vortex toward Eurasia (Fig. 10a). Note that blocking over the Ural Mountains can also make a significant contribution to surface cooling anomalies (Zhang et al. 2016). For NA events, the surface cooling anomalies over North America (Fig. 10b) are not only related to the negative height anomalies induced by the polar vortex shift toward North America but also to blocking over the Bering Strait. In addition, the surface cooling anomalies over parts of Eurasia may be a result of the elongation of the polar vortex (Fig. 1b). For ATL events, statistically significant surface cooling anomalies over the northern Atlantic (Fig. 10c) are closely associated with the negative height anomalies induced by the polar vortex shift toward the North Atlantic. The differences in the patterns of SAT anomalies during the polar vortex shift events with small and large deformation are consistent with the differences in the corresponding patterns of height anomalies.

6. Conclusions

This study, based on the ERA-Interim dataset, uses a composite approach to analyze the preconditions for the stratospheric polar vortex shift events toward Eurasia (EUR), North America (NA), and the Atlantic (ATL). For EUR events, the zonal wave-1 geopotential height anomalies have a positive center over North America and a negative center over Eurasia in the stratosphere before the central date. The anomalous wave-1 patterns are shown to be related to increased tropospheric blocking frequency over northern Europe and decreased frequency over the Bering Strait. The amplitude of negative zonal wave-2 heat flux anomalies into the lower stratosphere in EUR events with small polar vortex deformation is smaller than that in EUR events with large deformation.

For NA events, both zonal wave-1 and wave-2 geopotential height anomalies have a negative center over North America in the stratosphere before the central date. The patterns of anomalous zonal wave 1 and wave 2 at 10 hPa are opposite to those observed during the EUR events. The anomalous wave patterns are associated with increased tropospheric blocking frequency over the Bering Strait and decreased frequency over northern Europe. Note that the stratospheric polar vortex during NA events is more elongated than that of the other two types of events. In addition, the amplitude of the positive blocking frequency anomalies in NA events with large polar vortex deformation is larger than that in the events with small deformation, leading to a larger zonal wave-2 heat flux entering the lower stratosphere.

ATL events are similar to EUR events with enhanced wave-1 and reduced wave-2 activity, but the orientation of the wave-1 activity is more closely centered over the Atlantic. The anomalous wave patterns are related to increased tropospheric blocking frequency over the eastern North Atlantic and decreased frequency over the Bering Strait. In addition, the zonal wave-2 heat flux anomalies change from positive to negative prior to ATL events with large polar vortex deformation but not during the events with small deformation.

Our analysis reveals that the likelihood of the stratospheric polar vortex shift toward Eurasia, North America, and the Atlantic on the 850-K isentropic surface is increased in the presence of the blocking events with the spatial patterns of blocking frequency anomalies similar to those prior to EUR, NA, and ATL events. These shifts of the polar vortex toward Eurasia, North America, and the Atlantic lead to statistically significant negative height anomalies near the tropopause level and corresponding surface cooling anomalies over these three regions. Thus, the certain patterns of anomalous tropospheric blocking over northern Europe, the Bering Strait, and the eastern North Atlantic can be taken as the potential blocking precursors of the stratospheric polar vortex shifting toward Eurasia, North America, and the Atlantic.

It should be pointed out that the study mainly stresses the potential blocking precursors of the stratospheric polar vortex shift toward Eurasia, North America, and the Atlantic and pays no special attention to the role of the stratospheric conditions in the polar vortex shift events. Notably, the stratosphere itself also plays an important role in controlling the amount of planetary wave activity entering it from the troposphere (Scott and Polvani 2004; Cámara et al. 2017), and hence, impacts the vortex shift. An explosive growth of wave amplitude in the stratosphere, in some cases, does not result from the anomalous propagation of tropospheric planetary waves into the stratosphere but is the result of resonant wave amplification in the stratosphere, such as the vortex split of January 2009 (Albers and Birner 2014). Tripathi et al. (2016) also demonstrated that there is still only limited skill in the forecast of SSWs, even for those models with reasonable skill in forecasting the tropospheric blocking, implying that improved forecasts for the stratospheric polar vortex position require improved knowledge and representation of both the tropospheric blocking patterns and stratospheric state. How and to what extent the stratospheric state impacts the vortex position is beyond the scope of this study and is worthy of investigation in the future.

Acknowledgments. This work is supported by the National Natural Science Foundation of China (Grants 41630421, 41575038, 41521004, and 41705022). We greatly appreciate two anonymous reviewers and an editor for their constructive comments and suggestions. We thank the scientific teams at ECMWF for providing the reanalysis data.

REFERENCES

Albers, J. R., and T. Birner, 2014: Vortex preconditioning due to planetary and gravity waves prior to sudden stratospheric warmings. *J. Atmos. Sci.*, **71**, 4028–4054, https://doi.org/10.1175/JAS-D-14-0026.1.

Andrews, D. G., and M. E. McIntyre, 1976: Planetary waves in horizontal and vertical shear: The generalized Eliassen–Palm relation and the mean zonal acceleration. *J. Atmos. Sci.*, **33**, 2031–2048, https://doi.org/10.1175/1520-0469(1976)033<2031:PWIHAV>2.0.CO;2.

Attard, H. E., R. Rios-Berrios, C. T. Guastini, and A. L. Lang, 2016: Tropospheric and stratospheric precursors to the January 2013 sudden stratospheric warming. *Mon. Wea. Rev.*, **144**, 1321–1339, https://doi.org/10.1175/MWR-D-15-0175.1.

Baldwin, M. P., and T. J. Dunkerton, 1999: Propagation of the Arctic Oscillation from the stratosphere to the troposphere. *J. Geophys. Res.*, **104**, 30 937–30 946, https://doi.org/10.1029/1999JD900445.

——, and ——, 2001: Stratospheric harbingers of anomalous weather regimes. *Science*, **294**, 581–584, https://doi.org/10.1126/science.1063315.

Bancalá, S., K. Krüger, and M. Giorgetta, 2012: The preconditioning of major sudden stratospheric warmings. *J. Geophys. Res.*, **117**, D04101, https://doi.org/10.1029/2011JD016769.

Bao, M., X. Tan, D. L. Hartmann, and P. Ceppi, 2017: Classifying the tropospheric precursor patterns of sudden stratospheric warmings. *Geophys. Res. Lett.*, **44**, 8011–8016, https://doi.org/10.1002/2017GL074611.

Barriopedro, D., and N. Calvo, 2014: On the relationship between ENSO, stratospheric sudden warmings, and blocking. *J. Climate*, **27**, 4704–4720, https://doi.org/10.1175/JCLI-D-13-00770.1.

Cámara, A. D. L., J. R. Albers, T. Birner, R. R. Garcia, P. Hitchcock, D. E. Kinnison, and A. K. Smith, 2017: Sensitivity of sudden stratospheric warmings to previous stratospheric conditions. *J. Atmos. Sci.*, **74**, 2857–2877, https://doi.org/10.1175/JAS-D-17-0136.1.

Castanheira, J. M., and D. Barriopedro, 2010: Dynamical connection between tropospheric blockings and stratospheric polar vortex. *Geophys. Res. Lett.*, **37**, L13809, https://doi.org/10.1029/2010GL043819.

Charlton, A. J., and L. M. Polvani, 2007: A new look at stratospheric sudden warmings. Part I: Climatology and modeling benchmarks. *J. Climate*, **20**, 449–469, https://doi.org/10.1175/JCLI3996.1.

Charney, J. G., and P. G. Drazin, 1961: Propagation of planetary-scale disturbances from the lower into the upper atmosphere. *J. Geophys. Res.*, **66**, 83–109, https://doi.org/10.1029/JZ066i001p00083.

Cohen, J., and C. Fletcher, 2007: Improved skill of Northern Hemisphere winter surface temperature predictions based on land–atmosphere fall anomalies. *J. Climate*, **20**, 4118–4132, https://doi.org/10.1175/JCLI4241.1.

Dai, Y., and B. Tan, 2016: The western Pacific pattern precursor of major stratospheric sudden warmings and the ENSO modulation. *Environ. Res. Lett.*, **11**, 124032, https://doi.org/10.1088/1748-9326/aa538a.

Davini, P., C. Cagnazzo, S. Gualdi, and A. Navarra, 2012: Bidimensional diagnostics, variability, and trends of Northern Hemisphere blocking. *J. Climate*, **25**, 6496–6509, https://doi.org/10.1175/JCLI-D-12-00032.1.

——, ——, and J. A. Anstey, 2014: A blocking view of the stratosphere-troposphere coupling. *J. Geophys. Res. Atmos.*, **119**, 11 100–11 115, https://doi.org/10.1002/2014JD021703.

Dee, D. P., and Coauthors, 2011: The ERA-Interim reanalysis: Configuration and performance of the data assimilation system. *Quart. J. Roy. Meteor. Soc.*, **137**, 553–597, https://doi.org/10.1002/qj.828.

ECMWF, 2009: ERA-Interim project. National Center for Atmospheric Research Computational and Information Systems Laboratory Research Data Archive, accessed 13 May 2017, https://doi.org/10.5065/D6CR5RD9.

Garfinkel, C. I., and D. L. Hartmann, 2008: Different ENSO teleconnections and their effects on the stratospheric polar vortex. *J. Geophys. Res.*, **113**, D18114, https://doi.org/10.1029/2008JD009920.

——, S.-W. Son, K. Song, V. Aquila, and L. D. Oman, 2017: Stratospheric variability contributed to and sustained the recent hiatus in Eurasian winter warming. *Geophys. Res. Lett.*, **44**, 374–382, https://doi.org/10.1002/2016GL072035.

Hitchcock, P., and I. R. Simpson, 2014: The downward influence of stratospheric sudden warmings. *J. Atmos. Sci.*, **71**, 3856–3876, https://doi.org/10.1175/JAS-D-14-0012.1.

——, and P. H. Haynes, 2016: Stratospheric control of planetary waves. *Geophys. Res. Lett.*, **43**, 11 884–11 892, https://doi.org/10.1002/2016GL071372.

Hoskins, B. J., M. E. McIntyre, and A. W. Robertson, 1985: On the use and significance of isentropic potential vorticity maps. *Quart. J. Roy. Meteor. Soc.*, **111**, 877–946, https://doi.org/10.1002/qj.49711147002.

Huang, J., W. Tian, J. Zhang, Q. Huang, H. Tian, and J. Luo, 2017: The connection between extreme stratospheric polar vortex events and tropospheric blockings. *Quart. J. Roy. Meteor. Soc.*, **143**, 1148–1164, https://doi.org/10.1002/qj.3001.

Iza, M., and N. Calvo, 2015: Role of stratospheric sudden warmings on the response to central Pacific El Niño. *Geophys. Res. Lett.*, **42**, 2482–2489, https://doi.org/10.1002/2014GL062935.

Kidston, J., A. A. Scaife, S. C. Hardiman, D. M. Mitchell, N. Butchart, M. P. Baldwin, and L. J. Gray, 2015: Stratospheric influence on tropospheric jet streams, storm tracks and surface weather. *Nat. Geosci.*, **8**, 433–440, https://doi.org/10.1038/ngeo2424.

Kim, B.-M., S.-W. Son, S.-K. Min, J.-H. Jeong, S.-J. Kim, X. Zhang, T. Shim, and J.-H. Yoon, 2014: Weakening of the stratospheric polar vortex by Arctic sea-ice loss. *Nat. Commun.*, **5**, 4646, https://doi.org/10.1038/ncomms5646.

Kolstad, E. W., and A. J. Charlton-Perez, 2011: Observed and simulated precursors of stratospheric polar vortex anomalies in the Northern Hemisphere. *Climate Dyn.*, **37**, 1443–1456, https://doi.org/10.1007/s00382-010-0919-7.

——, T. Breiteig, and A. A. Scaife, 2010: The association between stratospheric weak polar vortex events and cold air outbreaks

in the Northern Hemisphere. *Quart. J. Roy. Meteor. Soc.*, **136**, 886–893, https://doi.org/10.1002/qj.620.

Kuroda, Y., 2008: Effect of stratospheric sudden warming and vortex intensification on the tropospheric climate. *J. Geophys. Res.*, **113**, D15110, https://doi.org/10.1029/2007JD009550.

Li, Y., and W. Tian, 2017: Different impact of central Pacific and eastern Pacific El Niño on the duration of sudden stratospheric warming. *Adv. Atmos. Sci.*, **34**, 771–782, https://doi.org/10.1007/s00376-017-6286-0.

——, ——, F. Xie, Z. Wen, J. Zhang, D. Hu, and Y. Han, 2018: The connection between the second leading mode of the winter North Pacific sea surface temperature anomalies and stratospheric sudden warming events. *Climate Dyn.*, https://doi.org/10.1007/s00382-017-3942-0, in press.

Limpasuvan, V., D. W. J. Thompson, and D. L. Hartmann, 2004: The life cycle of the Northern Hemisphere sudden stratospheric warmings. *J. Climate*, **17**, 2584–2596, https://doi.org/10.1175/1520-0442(2004)017<2584:TLCOTN>2.0.CO;2.

——, D. L. Hartmann, D. W. J. Thompson, K. Jeev, and Y. L. Yung, 2005: Stratosphere-troposphere evolution during polar vortex intensification. *J. Geophys. Res.*, **110**, D24101, https://doi.org/10.1029/2005JD006302.

Martineau, P., and S.-W. Son, 2013: Planetary-scale wave activity as a source of varying tropospheric response to stratospheric sudden warming events: A case study. *J. Geophys. Res. Atmos.*, **118**, 10 994–11 006, https://doi.org/10.1002/jgrd.50871.

——, and ——, 2015: Onset of circulation anomalies during stratospheric vortex weakening events: The role of planetary-scale waves. *J. Climate*, **28**, 7347–7370, https://doi.org/10.1175/JCLI-D-14-00478.1.

Martius, O., L. M. Polvani, and H. C. Davies, 2009: Blocking precursors to stratospheric sudden warming events. *Geophys. Res. Lett.*, **36**, L14806, https://doi.org/10.1029/2009GL038776.

Matsuno, T., 1970: Vertical propagation of stationary planetary waves in the winter Northern Hemisphere. *J. Atmos. Sci.*, **27**, 871–883, https://doi.org/10.1175/1520-0469(1970)027<0871:VPOSPW>2.0.CO;2.

Matthewman, N. J., and J. G. Esler, 2011: Stratospheric sudden warmings as self-tuning resonances. Part I: Vortex splitting events. *J. Atmos. Sci.*, **68**, 2481–2504, https://doi.org/10.1175/JAS-D-11-07.1.

——, ——, A. J. Charlton-Perez, and L. M. Polvani, 2009: A new look at stratospheric sudden warmings. Part III: Polar vortex evolution and vertical structure. *J. Climate*, **22**, 1566–1585, https://doi.org/10.1175/2008JCLI2365.1.

Maycock, A. C., and P. Hitchcock, 2015: Do split and displacement sudden stratospheric warmings have different annular mode signatures? *Geophys. Res. Lett.*, **42**, 10 943–10 951, https://doi.org/10.1002/2015GL066754.

Mitchell, D. M., L. J. Gray, J. Anstey, M. P. Baldwin, and A. J. Charlton-Perez, 2013: The influence of stratospheric vortex displacements and splits on surface climate. *J. Climate*, **26**, 2668–2682, https://doi.org/10.1175/JCLI-D-12-00030.1.

Morris, G. A., and Coauthors, 1995: Trajectory mapping and applications to data from the Upper Atmosphere Research Satellite. *J. Geophys. Res.*, **100**, 16 491–16 505, https://doi.org/10.1029/95JD01072.

Mukougawa, H., and T. Hirooka, 2004: Predictability of stratospheric sudden warming: A case study for 1998/99 winter. *Mon. Wea. Rev.*, **132**, 1764–1776, https://doi.org/10.1175/1520-0493(2004)132<1764:POSSWA>2.0.CO;2.

Nash, E. R., P. A. Newman, J. E. Rosenfield, and M. R. Schoeberl, 1996: An objective determination of the polar vortex using Ertel's potential vorticity. *J. Geophys. Res.*, **101**, 9471–9478, https://doi.org/10.1029/96JD00066.

Nath, D., W. Chen, C. Zelin, A. I. Pogoreltsev, and K. Wei, 2016: Dynamics of 2013 sudden stratospheric warming event and its impact on cold weather over Eurasia: Role of planetary wave reflection. *Sci. Rep.*, **6**, 24174, https://doi.org/10.1038/srep24174.

Nishii, K., H. Nakamura, and Y. J. Orsolini, 2010: Cooling of the wintertime Arctic stratosphere induced by the western Pacific teleconnection pattern. *Geophys. Res. Lett.*, **37**, L13805, https://doi.org/10.1029/2010GL043551.

——, ——, and ——, 2011: Geographical dependence observed in blocking high influence on the stratospheric variability through enhancement and suppression of upward planetary-wave propagation. *J. Climate*, **24**, 6408–6423, https://doi.org/10.1175/JCLI-D-10-05021.1.

Plumb, R. A., 1985: On the three-dimensional propagation of stationary waves. *J. Atmos. Sci.*, **42**, 217–229, https:/doi.org/10.1175/1520-0469(1985)042,0217:OTTDPO.2.0.CO;2.

Polvani, L. M., and D. W. Waugh, 2004: Upward wave activity flux as a precursor to extreme stratospheric events and subsequent anomalous surface weather regimes. *J. Climate*, **17**, 3548–3554, https://doi.org/10.1175/1520-0442(2004)017<3548:UWAFAA>2.0.CO;2.

——, L. Sun, A. H. Butler, J. H. Richter, and C. Deser, 2017: Distinguishing stratospheric sudden warmings from ENSO as key drivers of wintertime climate variability over the North Atlantic and Eurasia. *J. Climate*, **30**, 1959–1969, https://doi.org/10.1175/JCLI-D-16-0277.1.

Quiroz, R. S., 1986: The association of stratospheric warmings with tropospheric blocking. *J. Geophys. Res.*, **91**, 5277–5285, https://doi.org/10.1029/JD091iD04p05277.

Scott, R. K., and L. M. Polvani, 2004: Stratospheric control of upward wave flux near the tropopause. *Geophys. Res. Lett.*, **31**, L02115, https://doi.org/10.1029/2003GL017965.

Seviour, W. J. M., 2017: Weakening and shift of the Arctic stratospheric polar vortex: Internal variability or forced response? *Geophys. Res. Lett.*, **44**, 3365–3373, https://doi.org/10.1002/2017GL073071.

——, D. M. Mitchell, and L. J. Gray, 2013: A practical method to identify displaced and split stratospheric polar vortex events. *Geophys. Res. Lett.*, **40**, 5268–5273, https://doi.org/10.1002/grl.50927.

——, L. J. Gray, and D. M. Mitchell, 2016: Stratospheric polar vortex splits and displacements in the high-top CMIP5 climate models. *J. Geophys. Res. Atmos.*, **121**, 1400–1413, https://doi.org/10.1002/2015JD024178.

Smith, K. L., C. G. Fletcher, and P. J. Kushner, 2010: The role of linear interference in the annular mode response to extratropical surface forcing. *J. Climate*, **23**, 6036–6050, https://doi.org/10.1175/2010JCLI3606.1.

Taguchi, M., and D. L. Hartmann, 2006: Increased occurrence of stratospheric sudden warmings during El Niño as simulated by WACCM. *J. Climate*, **19**, 324–332, https://doi.org/10.1175/JCLI3655.1.

Thompson, D. W. J., M. P. Baldwin, and J. M. Wallace, 2002: Stratospheric connection to Northern Hemisphere wintertime weather: Implications for prediction. *J. Climate*, **15**, 1421–1428, https://doi.org/10.1175/1520-0442(2002)015<1421:SCTNHW>2.0.CO;2.

Tripathi, O. P., and Coauthors, 2016: Examining the predictability of the stratospheric sudden warming of January 2013 using

multiple NWP systems. *Mon. Wea. Rev.*, **144**, 1935–1960, https://doi.org/10.1175/MWR-D-15-0010.1.

Wang, L., and W. Chen, 2010: Downward Arctic Oscillation signal associated with moderate weak stratospheric polar vortex and the cold December 2009. *Geophys. Res. Lett.*, **37**, L09707, https://doi.org/10.1029/2010GL042659.

Wilks, D. S., 2016: ''The stippling shows statistically significant grid points'': How research results are routinely overstated and overinterpreted, and what to do about it. *Bull. Amer. Meteor. Soc.*, **97**, 2263–2273, https://doi.org/10.1175/BAMS-D-15-00267.1.

Woollings, T., A. Charlton-Perez, S. Ineson, A. G. Marshall, and G. Masato, 2010: Associations between stratospheric variability and tropospheric blocking. *J. Geophys. Res.*, **115**, D06108, https://doi.org/10.1029/2009JD012742.

Xie, F., and Coauthors, 2016: A connection from Arctic stratospheric ozone to El Niño-Southern Oscillation. *Environ. Res. Lett.*, **11**, 124026, https://doi.org/10.1088/1748-9326/11/12/124026.

Zhang, J., W. Tian, M. P. Chipperfield, F. Xie, and J. Huang, 2016: Persistent shift of the Arctic polar vortex towards the Eurasian continent in recent decades. *Nat. Climate Change*, **6**, 1094–1099, https://doi.org/10.1038/nclimate3136.

——, and Coauthors, 2018: Stratospheric ozone loss over the Eurasian continent induced by the polar vortex shift. *Nat. Commun.*, **9**, 206, https://doi.org/10.1038/s41467-017-02565-2.

Zwiers, F. W., and H. von Storch, 1995: Taking serial correlation into account in tests of the mean. *J. Climate*, **8**, 336–351, https://doi.org/10.1175/1520-0442(1995)008<0336:TSCIAI>2.0.CO;2.